

Two-dimensional topological superconductivity in Pb/Co/Si(111)

Gerbold C. Ménard¹, Sébastien Guissart², Christophe Brun¹, Mircea Trif², François Debontridder¹, Raphaël T. Leriche¹, Dominique Demaille¹, Dimitri Roditchev^{1,3}, Pascal Simon^{2,*} and Tristan Cren^{1†}

¹*Institut des Nanosciences de Paris,*

Université Pierre et Marie Curie (UPMC),

CNRS-UMR 7588, 4 place Jussieu, 75252 Paris, France

²*Laboratoire de Physique des Solides, CNRS, Univ. Paris-Sud,*

Université Paris-Saclay, 91405 Orsay Cedex, France and

³*Laboratoire de physique et d'étude des matériaux,*

LPEM-UMR8213/CNRS-ESPCI ParisTech-UPMC,

10 rue Vauquelin, 75005 Paris, France

(Dated: July 10, 2022)

Abstract

Just like insulators can host topological Dirac states at their edges, superconductors can also exhibit topological phases characterized by Majorana edge states. Remarkable zero-energy states have been recently observed at the two ends of proximity induced superconducting wires [1, 2], and were interpreted as localized Majorana end states in one-dimensional (1D) topological superconductor. By contrast, propagating Majorana states should exist at the 1D edges of two-dimensional (2D) topological superconductors. Here we report the direct observation of dispersive in-gap states surrounding topological superconducting domains made of a single atomic layer of Pb covering magnetic islands of Co/Si(111). We interpret the observed continuous dispersion across the superconducting gap in terms of a spatial topological transition accompanied by a chiral edge mode and residual gaped helical edge states. Our experimental approach enables the engineering and control of a large variety of novel quantum phases. This opens new horizons in the field of quantum materials and quantum electronics where the magnetization of the domains could be used as a control parameter for the manipulation of topological states.

Superconductors with a fully opened gap can be labeled by some integer numbers according to the classification of non-interacting topological insulators and superconductors [3, 4]. In 2D time-reversal invariant superconductors, the topological properties can be characterized by a \mathbb{Z}_2 invariant (0 or 1) that separates the trivial phases from the topological ones [5, 6]. When time-reversal symmetry (TRS) is broken, several topological phases are possible and characterized by an integer number \mathbb{Z} corresponding to the number of Majorana chiral edge modes [5, 6].

In the search of two-dimensional topological superconductivity we focused on a monolayer of Pb/Si(111). This system is known to present strong spin-orbit coupling [7] that could potentially lead to topological p-wave superconductivity through Rashba spin-orbit interaction [8, 9]. The existence of very high in-plane critical fields in monolayer Pb/GaAs(110) [10], a similar system, indeed indicates the presence of an hybrid singlet-triplet order parameter with a strong triplet component. However, as pointed out by the absence of edge states at the interface between trivial Pb islands and the Pb/Si(111) monolayer this system is not topological on its own [11]. There is therefore a need for an additional ingredient for this system to enter a topological regime and among all possibilities local magnetism is probably the most promising one.

Point-like magnetic impurities in superconductors give rise to Shiba bound states [12, 13] which have been shown to possess a long-range spatial extent in 2D [14, 15]. On the other hand, arrays of magnetic impurities are predicted to give rise to chiral topological superconductivity [16–18], and the presence of a strong spin-orbit coupling may actually enhance this tendency [19]. In the following, we show that the local exchange magnetic field created by a magnetic domain locally triggers the transition between trivial and topological superconductivity.

We studied Pb/Si(111) monolayers with embedded Co/Si(111) magnetic domains (see Fig. 1.a). The samples are grown by self-assembly and sequential evaporation of Co and Pb on Si before annealing (see Methods). The final result is the obtention of a Pb monolayer covering subsurface Co-Si domains with diameters ranging between 5 and 10 nm randomly distributed all over the sample (see supplementary materials). The top Pb layer reconstructs into the stripped incommensurate phase (see Fig. 1.c) which has a coverage of approximately 1.3 ML, a critical temperature of 1.8 K and a gap $\Delta = 0.35$ meV [20]. In order to investigate the superconducting order and topological transitions we performed scanning tunneling

spectroscopy experiments with a superconducting tip at 300 mK.

On large scale tunneling conductance maps measured at the Fermi level, we observe very peculiar ring shaped structures shown in Fig. 1.b of the same size as the subsurface Co-Si domains. The thickness of the circle seen at E_F is approximately 0.7 nm which is comparable to the typical atomic dimensions and Fermi wavelength of the system [21]. This extension is much smaller than both the coherence length ξ ($\simeq 50$ nm) and the mean free path ℓ ($\simeq 4$ nm) of Pb/Si(111) [7]. This is remarkable since for superconductors in the diffusive limit $\ell \ll \xi$, the typical length scale of superconducting variations is given by the coherence length ξ . This fact suggests that these in-gap states are prevented to propagate inside or outside the ring in the same way surface states are confined in the case of topological insulators. The sharp circles we observe can then be traced back to Majorana edge states surrounding a topological domain. These states appear due to the topological transition stimulated by the underlying magnetic cluster that defines two areas, a topological one inside the cluster and a trivial one outside.

By expanding the measurement energy at finite bias inside the gap, the sharp line seen at zero bias splits into two circles, one moving inward, the other moving outward (see Fig. 1.d.-f.). Another important feature observed at $|V| \lesssim \Delta$ is that the sensitivity to disorder increases as the bias is moved towards the gap energy and the edge states get closer to the bulk states (Figs. 1.e.-f.). To better grasp the energy and space behaviour of these states we present on fig. 1.g a line-cut of the dI/dV maps deconvoluted from the superconducting tip (see supplementary materials S1) passing through the center of the topological disk as a function of energy. This conductance profile highlights the crossing of the states connecting both sides of the superconducting effective gap ± 0.3 meV. The X-shape of the dispersion in real space clearly shows that there is no anti-crossing at the Fermi energy. This absence of anti-crossing further calls for the topological nature of these boundary states.

Our experimental results suggest that we combine aspects of both chiral and helical superconductors. On one hand, the magnetic particle should favor a chiral behavior by leaving only one interface state (see supplementary materials S3). On the other hand, what we observe experimentally would be more compatible with an helical superconductor breaking TRS, which should allow the two states to spatially split (note that in a perfectly time-reversal invariant system the two helical states are spatially degenerate at all energies). The simplest interpretation of our experimental findings is to consider that our Pb/Si(111) mono-

layer is a trivial superconductor with some degree of triplet p-wave pairing [7] which evolves into a topological state by means of a magnetic Zeeman field created by the underlying cobalt cluster. TRS is thus broken in the vicinity of the cluster favouring a chiral behaviour. However, as shown theoretically in the supplementary material there is a reminiscence of helical superconductivity in such a case.

In order to substantiate this interpretation, we consider the following minimal Hamiltonian which carries the necessary ingredients to explain the experimental data:

$$\begin{aligned}
H = & [(p^2/2m - \mu) + \alpha(\mathbf{p} \times \boldsymbol{\sigma})_z] \tau_z + V_z(\mathbf{r})\sigma_z \\
& + [\Delta_S + (\Delta_T/k_F)(\mathbf{p} \times \boldsymbol{\sigma})_z] \tau_x
\end{aligned} \tag{1}$$

where the first and second terms stand for the kinetic and the Rashba spin-orbit interaction, with m the effective electron mass and α the strength of the spin-orbit interaction. The third term is the magnetic exchange coupling caused by the Co cluster which we describe as a spatially varying Zeeman term, while the fourth and fifth terms describe the s- and p-wave pairings, with strengths Δ_S and Δ_T , respectively (see supplementary S3 for details). Here $\boldsymbol{\sigma} = (\sigma_x, \sigma_y, \sigma_z)$ and $\boldsymbol{\tau} = (\tau_x, \tau_y, \tau_z)$ are Pauli matrices that act in the spin and Nambu (particle-hole) space respectively.

To simplify the discussion, we first set $\alpha = 0$; the general case is treated in the supplementary materials (S3) without qualitative changes. We also consider a constant out-of-plane Zeeman field $V_z(\mathbf{r}) \equiv V_z$, though our conclusion remains unchanged for a magnetic field with in-plane components (see supplementary Materials S3). The phase diagram of this model is shown in Fig. 2.a. The dashed lines illustrate the topological transitions where the superconducting gap closes. When $V_z = 0$, the system respects TRS and a topological transition between a trivial state and a helical state appears at $\Delta_T > \Delta_S$. Due to the different topological indices between a topological superconductor and the vacuum, a pair of helical edge states will appear when H is diagonalized on a semi-infinite plane for $\Delta_T > \Delta_S$ (see inset of Fig. 2.a): these states are Majorana dispersive fermions [5, 6]. Experimentally, we found no evidence of topological superconductivity far away from the magnetic cluster (no edge modes at the interface with bulk Pb [11]) which implies $\Delta_T < \Delta_S$ in our model. The superconducting gap measured in the Pb/Si(111) monolayer far away from the magnetic cluster $\Delta \sim 0.3$ meV should correspond to the effective gap $\Delta = \sqrt{\Delta_S^2 - \Delta_T^2}$.

Applying a magnetic field V_z breaks TRS. Surprisingly, we find that this does not destroy

the helical behaviour of the edges, but only makes these edges inequivalent, or (quasi-)helical, so that they are propagating with different velocities and can separate spatially. A second topological transition occurs at $V_z = \sqrt{\Delta_S^2 + \mu^2}$, after which the system becomes purely chiral. In this phase, only one propagating Majorana edge state exist. This is at odds with the helical case that exhibits a pair of states with opposite chiralities. Thus chiral superconductivity compares to quantum Hall effect in the same way as helical superconductivity compares to quantum spin Hall effect [5]. We should stress that the helical phase at $V_z \neq 0$ is only weakly topologically protected due to TRS breaking (see supplementary materials S4).

In order to simulate our experimental situation, we consider the Hamiltonian in Eq. (1) but now with an inhomogeneous magnetic field $V_z(r)$. We diagonalize H and compute the local density of states $\rho(E, r)$ at energy E and position r as measured by the STM tip. We assume that the cluster generates a strong Zeeman field which locally drives the system into a chiral topological superconducting phase. Taking a smooth profile for $V_z(r)$ (with a decay length of a few nm), moving away from the cluster thus realizes a continuous path in the phase diagram drawn in Fig. 2.a which goes from a chiral superconducting phase to the trivial one passing via some intermediate (quasi-)helical phase. Our numerical calculation for $\rho(E, r)$ is shown in Fig. 3.a. We find a qualitative agreement with our experimental data shown in Fig. 1.g. An important feature of our theoretical analysis is that the existence of a topological phase transition does not depend on any fine tuning of the parameters which only affect the fine details of the spatial dispersion. In Fig. 3.b, we show the dispersion relation with the momentum k_θ (conjugate to the perimeter of the magnetic disk) which is obtained by diagonalizing Eq. (1) for an abrupt step (with a decay length of the order of a few Å). The chiral Majorana edge state is clearly identified (in red) together with residual hybridized helical states. The X shaped real-space crossing (Fig. 1.d) can be interpreted within this Hamiltonian as a closure of topological gaps with associated dispersive Majorana edge states, the chiral Majorana mode being robust and topologically protected. Simulations of such system in the diffusive regime may offer a better quantitative description, however the use of Usadel equations to describe topological superconductivity remains an open issue.

In conclusion, by using a mixed p- and s-wave 2D superconductor coupled to a magnetic cluster we observed the realization of topological superconductivity through the appearance of circular edge states. The model we developed reproduces well the experiments without

any fine tuning of the parameters. The robustness of this model proves that it should be easily generalized to many other systems. Our discovery will be of major importance in the current development of quantum electronics based on the braiding of Majorana bound states. For such purpose one may use Majorana bound states in vortex cores in a 2D topological superconductor and in this context the method we developed is a decisive breakthrough. The two major advantages of this road map is that it is compatible with current Si technology, and that the length scale of the topological objects of several tens of nanometres is particularly interesting for concrete technological developments.

Methods *Sample preparation and characterization.* The 7×7 reconstructed n-Si(111) ($n \simeq 10^{19} \text{cm}^{-3}$) was prepared by direct current heating to $1,200^\circ\text{C}$ followed by an annealing procedure between 900°C and 500°C . Subsequently, 10^{-3} monolayers of Co were evaporated in 6 seconds on the Si(111)- 7×7 kept at room temperature, using an electron beam evaporator calibrated with a quartz micro-balance. 4 monolayers of Pb were then evaporated using another electron beam evaporator. The Pb overlayer was formed by annealing the sample at 375°C for 90 sec by direct current heating. This step leads to a stripped incommensurate (SIC) reconstruction of the Pb monolayer. At no stage of the sample preparation did the pressure exceed $P = 3.10^{-10}$ mbar. The scanning tunnelling spectroscopy measurements were performed in situ with a home-made apparatus at a base temperature of 280 mK and in ultrahigh vacuum in the low 10^{-11} mbar range. Mechanically sharpened Pt/Ir tips were used. These tips were made superconducting by crashing them into silicon carbides protrusions covered with Pb. The resulting superconducting gap of the tip was estimated to be 1.3 meV, close to bulk Pb. A bias voltage was applied to the sample with respect to the tip. Typical set-point parameters for topography are 20 pA at $V = -5$ mV. Typical set-point parameters for spectroscopy are 120 pA at $V = 5$ mV. The electron temperature was estimated to be 360 mK. The tunnelling conductance curves dI/dV were numerically differentiated from raw $I(V)$ experimental data. Each conductance map is extracted from a set of data consisting of spectroscopic $I(V)$ curves measured at each point of a 220×220 grid, acquired simultaneously with the topographic image. Each $I(V)$ curve contains 2000 energy points.

Acknowledgments. This work was supported by the French Agence Nationale de la Recherche through the contract ANR Mistral. G.C.M. acknowledges funding from the CFM

foundation providing his PhD grant.

Author contributions D.R., F.D. and T.C. built the experimental setup. G.C.M., C.B., R.T.L., D.D. and T.C. carried out the experiments. G.C.M. and T.C. processed and analysed the data. G.C.M., S.G., M.T., P.S. and T.C. performed the theoretical modeling while S.G. performed the numerical simulations. All authors discussed the results and participate in the writing of the manuscript.

* Electronic address: pascal.simon@u-psud.fr

† Electronic address: tristan.cren@upmc.fr

- [1] V. Mourik et al., *Signatures of Majorana fermions in hybrid superconductor-semiconductor nanowire devices*, Science **336**, 1003-1007 (2012).
- [2] S. Nadj-Perge et al., *Observation of Majorana Fermions in Ferromagnetic Atomic Chains on a Superconductor*, Science **346**, 6209 (2014).
- [3] A. P. Schnyder, S. Ryu, A. Furusaki, and A. W. W. Ludwig, *Classification of topological insulators and superconductors in three spatial dimensions*, Phys. Rev. B **78**, 195125 (2008); S. Ryu, A. P. Schnyder, A. Furusaki, A. W. W. Ludwig, *Topological insulators and superconductors: ten-fold way and dimensional hierarchy*, New Journal of Physics **12**, 065010 (2010).
- [4] A. Y. Kitaev, *Periodic table for topological insulators and superconductors*, AIP Conf. Proc. **1134**, 22 (2009).
- [5] X.-L. Qi and S.-C. Zhang, *Topological insulators and superconductors*, Rev. Mod. Phys. **83**, 1057-1110 (2011).
- [6] B. A. Bernevig and T. L. Huges, *Topological insulators and topological superconductors*, Princeton university press (2013).
- [7] C. Brun et al., *Remarkable effects of disorder on superconductivity of single atomic layers of lead on silico*, Nat. Phys. **10**, 444-450 (2014).
- [8] V. M. Édél'shtein, *Characteristics of the Cooper pairing in two-dimensional noncentrosymmetric electron systems*, Zh. Eksp. Teor. Fiz., **95**, 2151-2162 (1989).
- [9] L. P. Gor'kov and E. I. Rashba, *Superconducting 2D system with lifted spin degeneracy: mixed singlet-triplet state*, Phys. Rev. Lett., **87**, 037004 (2001).

- [10] T. Sekihara, R. Masutomi, and T. Okamoto, *Two-dimensional superconducting state of monolayer Pb films grown on GaAs(110) in a strong parallel magnetic field*, Phys. Rev. Lett. **111**, 057005 (2013).
- [11] V. Cherkez et al. *Proximity Effect between Two Superconductors Spatially Resolved by Scanning Tunneling Spectroscopy*, Phys. Rev. X, **4**, 011033 (2014).
- [12] A. V. Balatsky, I. Vekhter, and J.-X. Zhu, *Impurity-induced states in conventional and unconventional superconductors*, Rev. Mod. Phys. **78**, 373 (2006).
- [13] A. Yazdani, B. A. Jones, C. P. Lutz, M. F. Crommie, and D. M. Eigler, *Probing the Local Effects of Magnetic Impurities on Superconductivity*, Science **275**, 1767 (1997).
- [14] G. Ménard et al., *Coherent long-range magnetic bound states in a superconductor*, Nat. Phys. **11**, 1013-1017 (2015).
- [15] V. Kaladzhyan, C. Bena, and P. Simon, *Characterizing unconventional superconductors from the spin structure of impurity-induced bound states*, Phys. Rev. B **93**, 214514 (2016).
- [16] T.-P. Choy, J. M. Edge, A. R. Akhmerov, and C. W. J. Beenakker, *Majorana fermions emerging from magnetic nanoparticles on a superconductor without spin-orbit coupling*, Phys. Rev. B **84**, 195442 (2011).
- [17] S. Nakosai, Y. Tanaka, and N. Nagaosa, *Two-dimensional p-wave superconducting states with magnetic moments on a conventional s-wave superconductor*, Phys. Rev. B **88**, 180503 (2013).
- [18] S. Nadj-Perge, I. K. Drozdov, B. A. Bernevig, and A. Yazdani, *Proposal for realizing Majorana fermions in chains of magnetic atoms on a superconductor*, Phys. Rev. B **88**, 020407 (2013).
- [19] J. Roetynen and T. Ojanen, *Topological superconductivity and high Chern numbers in 2D ferromagnetic Shiba lattices*, Phys. Rev. Lett. **114**, 236803 (2015).
- [20] T. Zhang et al., *Superconductivity in one-atomic layer metal films grown on Si(111)*, Nat. Phys. **6**, 104-108 (2010).
- [21] W. H. Choi et al, *Electronic structure of dense Pb overlayers on Si(111) investigated using angle-resolved photoemission*, Phys. Rev. B **75**, 075329 (2007).
- [22] I. Gierz et al., *Silicon surface with giant spin splitting*, Phys. Rev. Lett. **103**, 046803 (2009)
- [23] J. H. Dil et al., *Rashba-type spin-orbit splitting of quantum well states in ultrathin Pb films*, Phys. Rev. Lett. **101**, 266802 (2008)
- [24] Oreg, Y. and Refael, G. and von Oppen, F., *Helical liquids and Majorana bound states in quantum wires*, Phys. Rev. Lett. **105**, 177002 (2010)

- [25] B. J. Powell and, J. F. Annett and B. L. Györfy *The gap equations for spin singlet and triplet ferromagnetic superconductors*, Journal of Physics A: Mathematical and General, **36**, 9289-9302 (2003).
- [26] K. Bjoernson and A. M. Black-Shaffer, *Probing vortex Majorana fermions and topology in semiconductor/superconductor heterostructures*, Phys. Rev. B, **97**, 214514 (2015).
- [27] M.-X. Wang and al., *The coexistence of superconductivity and topological order in the Bi_2Se_3 thin films*, Science, **336**, 52-55 (2015).
- [28] S.-Y. Xu and al., *Momentum-space imaging of Cooper pairing in a half-Dirac-gas topological superconductor*, Nat. Phys., **10**, 943-950 (2014).
- [29] X.-L. Qi and al., *Time-reversal-invariant topological superconductors and superfluids in two and three dimensions*, Phys. Rev. Lett., **102**, 187001 (2009).
- [30] C.-K. Lu and S. Yip, *Zero-energy vortex bound states in noncentrosymmetric superconductors*, Phys. Rev. B, **78**, 132502 (2008).

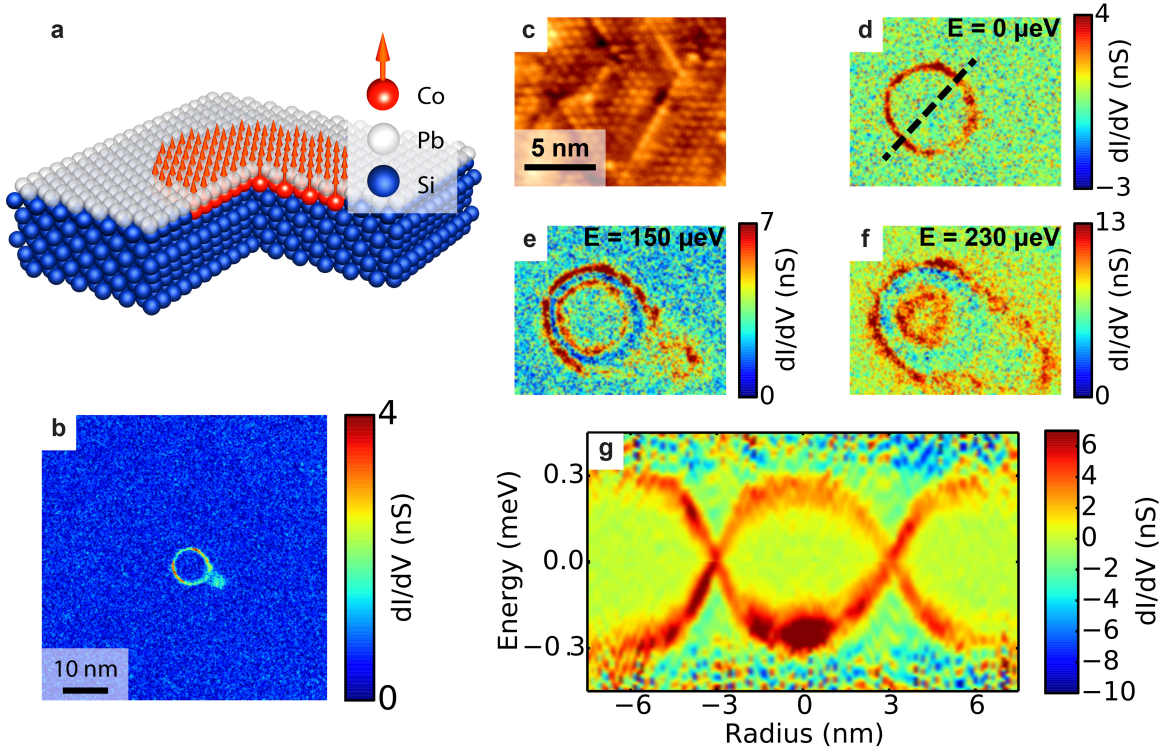


FIG. 1: **Scanning tunneling spectroscopy of topological edge states** : **a.** Schematic structure of the system investigated by STM. A monolayer of Pb is grown on top of Si(111) at the surface of which magnetic discs of Co were previously grown. **b.** Near zero-bias (integrated over 0.05 meV) conductance map of an area $63 \times 63 \text{ nm}^2$ showing the experimental observation of the edge states of a topological superconductor. Everywhere else the superconducting gap is perfectly conserved as evidenced by the homogeneous blue color. **c.** Topography of a $16 \times 13 \text{ nm}^2$ area showing the atomic structure of the Pb/Si(111) monolayer over the magnetic cluster. **b.-f.** Conductance maps of the same area at three different voltage biases ($0 \text{ } \mu\text{eV}$, $100 \text{ } \mu\text{eV}$, $200 \text{ } \mu\text{eV}$ respectively) showing the energy evolution of the edge states appearing at the frontier between a topological and a trivial superconductor. This area corresponds to the same region of the sample as the one shown on b. **g.** Line-cut of the conductance map plotted as a function of the distance from the centre of the disc and the energy. This image shows the spatial dispersion of the topological edge states across the interface ($\simeq \pm 3 \text{ nm}$) characterized by a X-shape crossing. The cut is taken along the black dashed line shown on d.

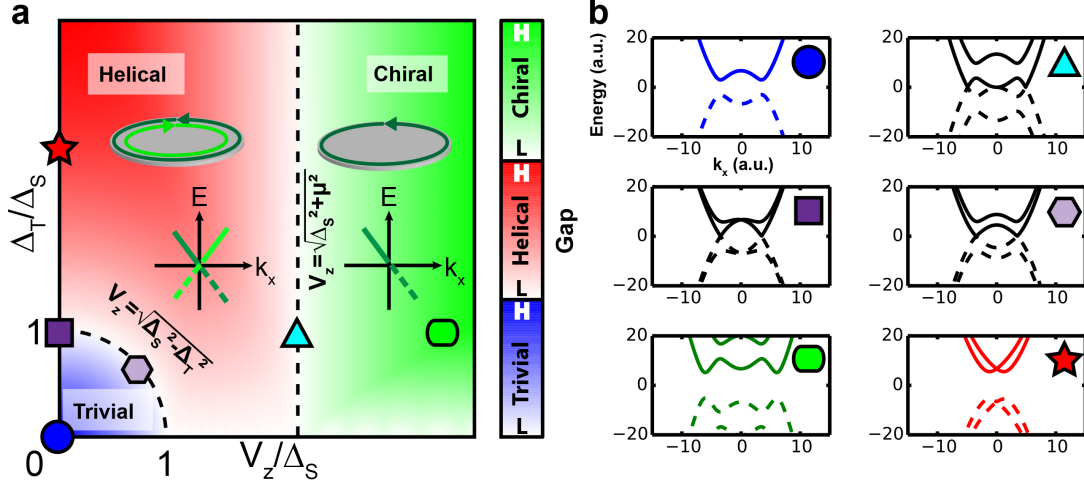


FIG. 2: **Topological transitions in superconductors:** **a.** Phase diagram of 2D topological superconductivity as a function of the Zeeman field V_z and the triplet order parameter amplitude Δ_T . The black dashed lines show the transitions between the trivial and helical phases as well as the transition between the helical and chiral phases. The insets show the typical behaviour of the edge states for the helical case (with two counter-propagating edge states) and the chiral case (only one edge state whose chirality is determined by the orientation of the magnetic field). The colour code corresponds to the values of the gap in each phase with one colour for each phase. **b.** Evolution of the band structure of a system with a parabolic dispersion for different values of the parameters V_z and Δ_T . The coloured symbols in each of the plot refers to the symbols in a, whose position in the phase diagram give the values of the parameters used for the computation of the dispersion.

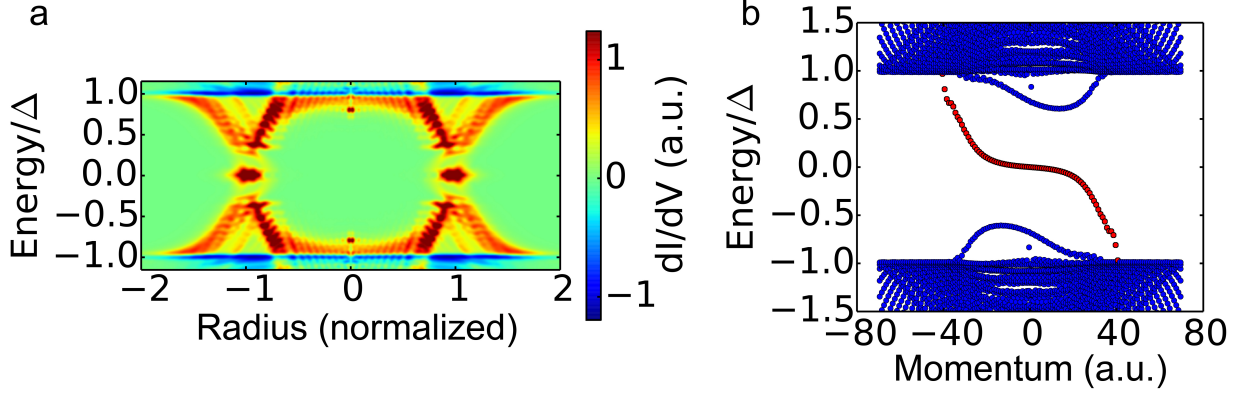


FIG. 3: **Theoretical calculation:** **a.** Real space tight binding calculation of $\rho(r, E)$. The parameters used for the calculation are a hopping amplitude $t = 50$, a chemical potential $\mu = 5$, a singlet order parameter amplitude $\Delta_S = 4$, a triplet order parameter amplitude $\Delta_T = 1.4$ for a spin-orbit coupling value $\alpha = 0$. The Zeeman potential $V_z(r)$ evolves smoothly from $V_z = 12$ to $V_z = 0$ over 30 sites. **b.** Spectrum $E(k_\theta)$ for a Zeeman potential $V_z(r)$ evolving from $V_z = 12$ to $V_z = 0$ over 3 sites. The other parameters are identical.